UNITED IMAGING

RSNA 2022 Edition

Issue Highlights

Quantitative assessment of AI-based chest CT lung nodule detection in lung cancer screening: future prospects and main challenges

Marufjon Salokhiddinov, et al.
Page 7

Performance evaluation of the artificial intelligence assisted compressed sensing MR technique in routine clinical settings

Adiraju Karthik, et al.
Page 16

Expert interview: Exploring the past, present, and future of total-body PET with Dr. Simon R. Cherry

Simon R. Cherry
Page 34

Future of radiology in developing countries

Harsh Mahajan and Vidur Mahajan
Page 60

Disclaimer

The articles contained in this magazine are provided solely by the authors, and the author(s) of each article appearing in this magazine is/are solely responsible for the content thereof as well as personal data, which is used anonymously or complied with applicable data privacy laws or regulations. United Imaging Healthcare makes no representation or warranties, expressly or impliedly, with respect to the accuracy, timeliness, reliability, legitimacy, applicability, fitness, originality, or completeness of the contents of this magazine. United Imaging Healthcare assumes no legal responsibility or liability for any error, omission, or illegality with respect to the material contained within.

All articles contained in this magazine only represent the opinions and views of the authors and do not implicitly or explicitly represent any official positions or policies, or medical opinions of United Imaging Healthcare or the institutions with which the authors are affiliated unless this is clearly specified. Discussions of any brand, services, or products in the magazine should not be construed as promotion or endorsement thereof.

Articles published in this magazine are intended to inspire further general scientific research, investigation, understanding, and discussion only and are NOT intended to and should not be relied upon as recommending or promoting a specific medical advice, method, diagnosis, or treatment by physicians for any particular individual, nor to replace the advice of a medical doctor or other healthcare professional. Any individual wishing to apply the information in this magazine for the purposes of improving their own health should not do so without consulting with a qualified medical practitioner. All patients need to be treated in an individual manner by their personal medical advisors. The decision to utilize any information in this magazine is ultimately at the sole discretion of the reader, who assumes full responsibility for any and all consequences arising from such a decision. United Imaging Healthcare makes no representations or warranties with respect to any treatment, action, or application of medication or preparation by any person following the information offered or provided within or through the magazine. United Imaging Healthcare shall remain free of any fault, liability, or responsibility for any loss or harm, whether real or perceived, resulting from the use of information in this magazine.

The articles included in this magazine may contain work in progress, which represents ongoing research and development. Such technologies are not available for sale in China or the United States for clinical use and also may not available for such sales in other countries around the world.

Please note that the magazine is intended to be distributed only within a limited scope instead of publication.

If you have any questions about the magazine, or simply wish to reach out to us for any other reasons, you are welcomed to contact us at the following email address: compliance@united-imaging.com

Systematic evaluation of advanced PET image reconstruction algorithms according to the Japanese standard criteria – a preliminary phantom study

Kenta Miwa[a1], Masanori Watanabe[b], Masanobu Ishiguro[b], Tensho Yamao[a], Akira Hirayama[c], Hiroshi Toyama[d]

[a]Department of Radiological Sciences, School of Health Sciences, Fukushima Medical University
[b]Department of Radiology, Fujita Health University Hospital
[c]United Imaging Healthcare Japan K.K.
[d]Department of Radiology, Fujita Health University School of Medicine

Abstract

HYPER Iterative (Regularized OSEM), uAI® HYPER DLR (Deep Learning Reconstruction), and uAI® HYPER DPR (Deep Progressive Reconstruction) are advanced PET image reconstruction algorithms that have recently been introduced into clinical practice in Japan. We systematically determined the performance of these algorithms by measuring various indices of image quality and quantitative accuracy according to the Japanese Society of Nuclear Medicine (JSNM) guidelines derived from images acquired using a uMI® 550 PET/CT system (United Imaging Healthcare, Shanghai, China). The image quality index ($Q_{H,10\ mm}/N_{10\ mm}$) obtained using HYPER Iterative, DLR and DPR satisfied the JSNM criterion of ≥ 2.5. The $Q_{H,10\ mm}/N_{10\ mm}$ value for HYPER DPR with Enhance2 containing non-local mean and Metz filters as a postfiltering option was 11.5, which was the best among the evaluated reconstruction methods. Sphere detectability, on the other hand, was better with HYPER DPR than with the other reconstruction methods assessed. Quantitation of 10 mm spheres was improved with HYPER Iterative, DLR and DPR compared to OSEM. Overall, our results showed that the advanced image reconstruction algorithms can improve image quality and quantitative accuracy (particularly in 10 mm spheres), compared with OSEM-based reconstruction methods which may improve detectability of smaller lesions. HYPER DPR reduced noise, improved image contrast, and enhanced PET image quantitation.

1. Background

Positron emission tomography/computed tomography (PET/CT) using ^{18}F-fluoro-2-deoxy-D-glucose (FDG) has become an essential tool for diagnosing and staging cancer. Furthermore, PET/CT imaging is becoming more important as a means of providing quantitative biomarkers for monitoring therapeutic responses and evaluating new drug therapies. However, PET image quality and quantitative accuracy can be sensitive to various factors such as imaging protocols, PET scanner specifications, reconstruction methods and parameters [1]. The Japanese Society of Nuclear Medicine (JSNM) has published standard PET imaging protocols together with phantom test procedures and criteria for oncological PET imaging using FDG. The executive summary is available on the JSNM website (http://jsnm.org/archives/3071/). The JSNM standards for image quality and quantitative accuracy are regularly updated to account for advancements in hardware and software performance of PET scanners to ensure harmonization of various scanner models, which can improve the robustness of multicenter studies.

The JSNM has recently published new standards for oncological FDG PET studies based on phantom data obtained from 23 PET/CT scanners primarily reconstructed using ordered subset expectation maximization (OSEM)-based reconstruction methods [2]. However, the image reconstruction results using the latest clinically available advanced image reconstruction algorithms – including

[1]Kenta Miwa and Tensho Yamao received financial funding through a sponsored research agreement between Fukushima Medical University and United Imaging Healthcare Japan.

HYPER Iterative (Regularized OSEM), and deep-learning (DL)-based methods such as uAI® HYPER DLR (Deep Learning Reconstruction) and uAI® HYPER DPR (Deep Progressive Reconstruction) were not included. Therefore, we systematically performed qualitative and quantitative evaluations of PET image reconstructions using these algorithms according to the JSNM phantom test guidelines.

2. Materials and Methods

2.1 PET/CT scanner

All PET data were acquired using a uMI® 550 PET/CT system (United Imaging Healthcare, Shanghai, China). The system is comprised of a PET scanner coupled to an 80-slice CT scanner. One detector block of the PET scanner is comprised of a 7 × 6 LYSO array of 2.76 × 2.76 × 16.3 mm^3 crystals coupled to silicon photomultiplier (SiPM) sensors. The uMI 550 has axial and transaxial fields of view (FOV) of 24 and 70 cm, respectively. The time-of-flight (TOF) timing resolution is 395 ps. The spatial resolution and sensitivity of the uMI 550 according to National Electrical Manufacturers Association (NEMA) NU 2-2018 standard are 2.95 mm/2.97 mm (transverse/axial) at 10 mm off center and 10.3 cps/kBq, respectively [3].

2.2 Phantom experiments

Phantom data were acquired according to the JSNM phantom test procedures [4]. We used a NEMA body phantom comprising six spheres with diameters of 10, 13, 17, 22, 28, and 37 mm. The sphere-to-background activity ratio (SBR) in the phantom was 4:1 with a background activity concentration of 2.53 kBq/mL.

2.3 Data acquisition and image reconstruction

We acquired PET images in three-dimensional list mode for 30 min and reconstructed them using OSEM + point spread function (PSF) + time-of-flight (TOF) (3 iterations; 20 subsets; postfilter, non-local mean and Gaussian filter 6 mm), HYPER Iterative (β values of 0.01, 0.07, 0.14, 0.21, 0.28, 0.35, 0.42, 0.49, 0.56, 0.63, 0.7, 0.77, 0.84, 0.91, and 0.98; PSF+TOF, on), HYPER DLR (2 iterations; 20 subsets; postfilter, combined non-local means, Gaussian and Metz filters, 4 mm; PSF+TOF, on), and HYPER DPR (smoothing strength, 1–5 (Smooth to Sharp); postfilter; combined non-local means; Gaussians and Metz filters, 4 mm; PSF+TOF, on). The reconstruction parameters for each algorithm were chosen to account for differences in convergence speeds to ensure that the algorithms were compared under optimal conditions, similar to our previous studies. The parameters for OSEM were derived from the existing clinical protocol at Fujita Health University Hospital; the parameters for HYPER DLR were based on the work performed by Xing *et al*. [5]; and the same Gaussian filter was used for both HYPER DLR and HYPER DPR for direct comparisons. Images were reconstructed in a 256 × 256 matrix, with a slice thickness of 2.68 mm. Data acquired in 30 min list mode were re-binned into acquisition durations of 2 and 10 min. All standard data corrections were applied.

2.4 Image analyses

We assessed image quality by evaluating the contrast of the 10 mm hot sphere and background variability on PET images acquired for 2 min using PMOD software version 3.8. A circular ROI was placed on the 10 mm sphere on an axial slice of the sphere center. We also placed twelve 10 mm diameter circular ROIs on the background on a slice of the sphere center and on slices ± 1 cm and ± 2 cm away from the center slice (60 ROIs total). The percent contrast (% contrast) for the 10 mm hot sphere ($Q_{H,10\,mm}$) was calculated as:

$$Q_{H,10\,mm} = \frac{C_{H,10\,mm}/C_{B,10\,mm} - 1}{a_H/a_B - 1} \times 100\ (\%),$$

where $C_{H,10\,mm}$ and $C_{B,10\,mm}$ are the average activity concentration in the ROI for the 10 mm sphere and in the background 10 mm diameter ROIs, respectively, and a_H/a_B is the known activity concentration ratio between the hot spheres and the background. The percent background variability ($N_{10\,mm}$) for the 10 mm circular ROIs was calculated as:

$$N_{10\,mm} = \frac{SD_{10\,mm}}{C_{B,10\,mm}} \times 100\ (\%), \text{ and}$$

$$SD_{10\,mm} = \sqrt{\frac{\sum_{k=1}^{K}\left(C_{B,10\,mm,k} - C_{B,10\,mm}\right)^2}{K-1}}, K = 60,$$

where $SD_{10\,mm}$ is the standard deviation of the mean activity concentration for the 60 background ROIs.

We assessed the quantitative accuracy of the data by measuring the mean standardized uptake value (SUV_{mean}), the relative recovery coefficient (RC) for the hot spheres, and the average SUV in the background ($SUV_{B,ave}$) on PET images acquired for 10 min.

3. Results

Figure 1 shows the % contrast, background variability, and image quality index ($Q_{H,10\ mm}$/ $N_{10\ mm}$) as a function of the β value in PET images reconstructed using HYPER Iterative.

The % contrast increased as the β value decreased. The % contrast was higher than that of OSEM + PSF + TOF at ranges of β = 0.01–0.70. Background variability decreased as the β value increased and was lower than that in OSEM + PSF + TOF when β = 0.63–0.98. The image quality index ($Q_{H,10\ mm}$/$N_{10\ mm}$) from HYPER Iterative satisfied the JSNM criterion of ≥ 2.5. The $Q_{H,10\ mm}$/$N_{10\ mm}$ value reached maximum at β = 0.63, then decreased as a function of increasing β values.

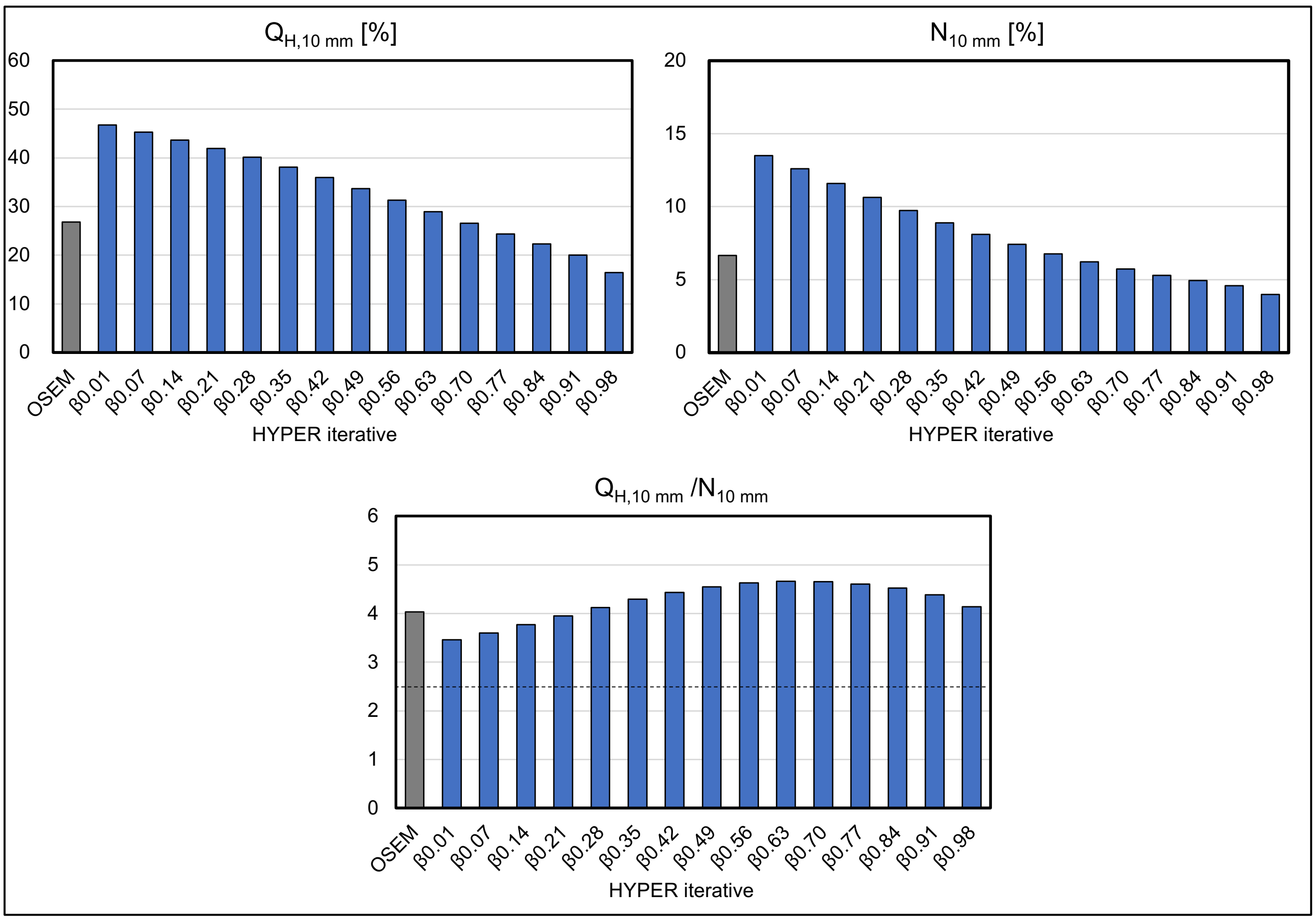

Figure 1. Percent contrast ($Q_{H,10\ mm}$), background variability ($N_{10\ mm}$), and image quality index ($Q_{H,10\ mm}$/ $N_{10\ mm}$) as a function of β in PET images reconstructed using HYPER Iterative. The dotted line represents the reference standards for the JSNM image quality acceptance. OSEM represents OSEM + PSF + TOF.

Figure 2 shows the % contrast, background variability, and image quality index ($Q_{H,10\ mm}$/$N_{10\ mm}$) with various postfilter options in PET images reconstructed using HYPER DLR. The % contrast in DLR was lower than that in OSEM + PSF + TOF without a postfilter. On the other hand, % contrast in DLR was almost identical to that in OSEM + PSF + TOF with a postfilter containing a non-local mean filter. The background variability was lower in DLR than in OSEM + PSF + TOF. Regardless, the image quality index ($Q_{H,10\ mm}$/$N_{10\ mm}$) in DLR satisfied the JSNM criterion for all configurations. The $Q_{H,10\ mm}$/$N_{10\ mm}$ values for DLR with Smooth1, Smooth3, and Enhance2 containing the non-local mean filter were higher than those of OSEM + PSF + TOF. The $Q_{H,10\ mm}$/$N_{10\ mm}$ value for DLR with Enhance2 was maximal among all configurations.

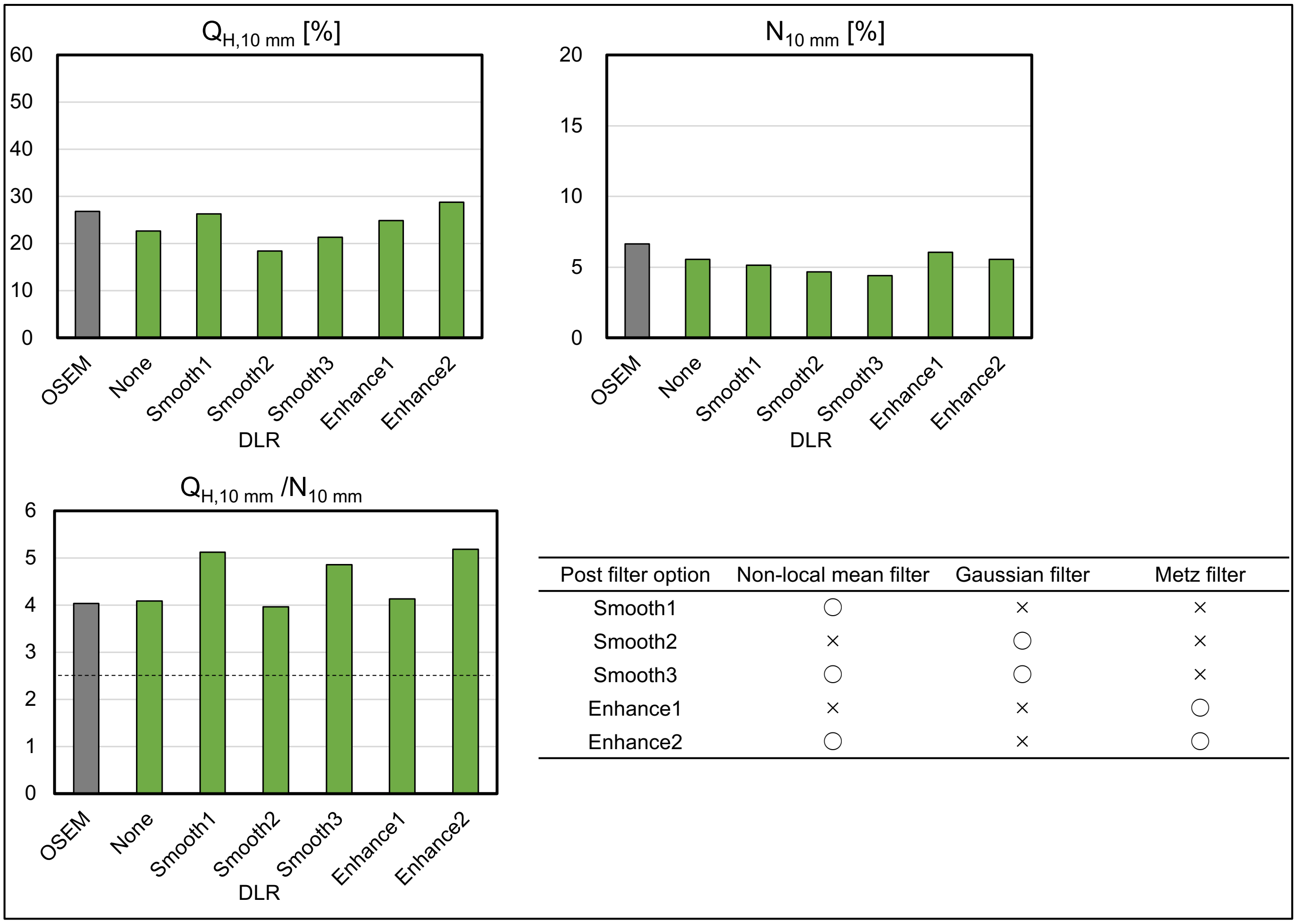

Post filter option	Non-local mean filter	Gaussian filter	Metz filter
Smooth1	○	×	×
Smooth2	×	○	×
Smooth3	○	○	×
Enhance1	×	×	○
Enhance2	○	×	○

Figure 2. Percent contrast, background variability, and quality index ($Q_{H,10\,mm}/N_{10\,mm}$) of PET images reconstructed using HYPER DLR with various postfilter options. The dotted line represents the reference standards for the JSNM image quality acceptance. OSEM represents OSEM + PSF + TOF; none represents no postfilter.

Figure 3 shows the % contrast, background variability, and image quality index ($Q_{H,10\,mm}/N_{10\,mm}$) with different smoothing strength and postfilter options in PET images reconstructed using HYPER DPR. The % contrast and background variability in DPR increased with increasing smoothing strength. The % contrast and background variability tended to be lower in DPR with Smooth2 and Smooth3 with a Gaussian filter, than in other postfilter options. The image quality index ($Q_{H,10\,mm}/N_{10\,mm}$) in DPR satisfied the JSNM criterion. The $Q_{H,10\,mm}/N_{10\,mm}$ values for DPR under all conditions were better than those for OSEM + PSF + TOF. The $Q_{H,10\,mm}/N_{10\,mm}$ values for DPR with Smooth1, Smooth3, and Enhance2 with a non-local mean filter were substantially better than those with other postfilter options. The $Q_{H,10\,mm}/N_{10\,mm}$ value for DPR with Enhance2 was maximal among all configurations.

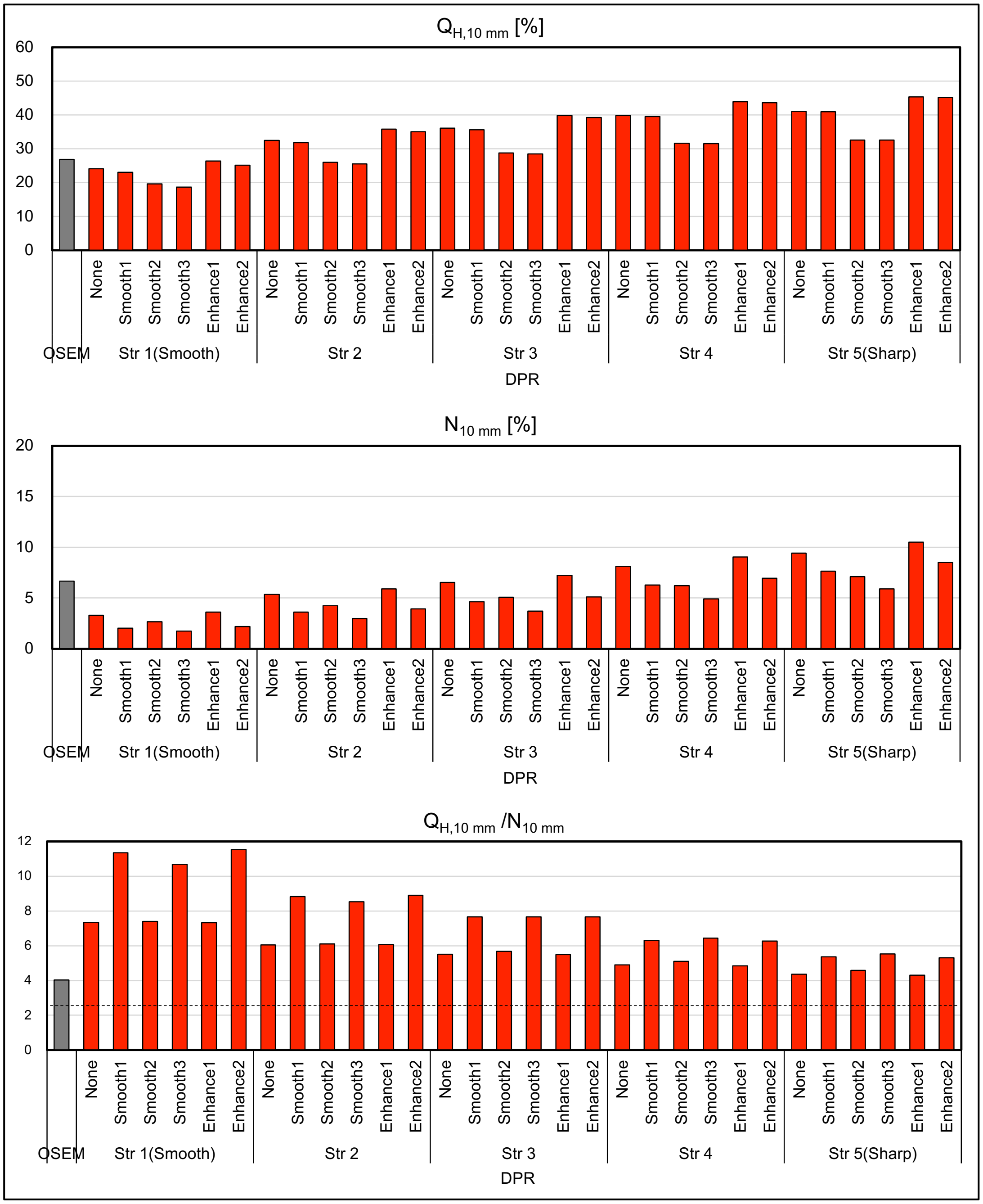

Figure 3. Percent contrast, background variability, and image quality index ($Q_{H,10\ mm}/N_{10\ mm}$) with different smoothing strength and postfilter options in DPR PET images. The dotted line represents the reference standards for the JSNM image quality acceptance. None represents no postfilter; OSEM represents OSEM + PSF + TOF; Str represents smoothing strength.

Figure 4 shows the relationship between % contrast and background variability for all reconstructed algorithms. The % contrast was plotted as a function of the background variability of hot spheres with diameters of 10 mm. Thus, a choice was needed between increased % contrast and decreased background variability. Ideally, these points on the graph would lie in the top left of the figure [6,7]. The balance between contrast and image noise was better in this descending order: HYPER DPR, HYPER Iterative, HYPER DLR, and OSEM.

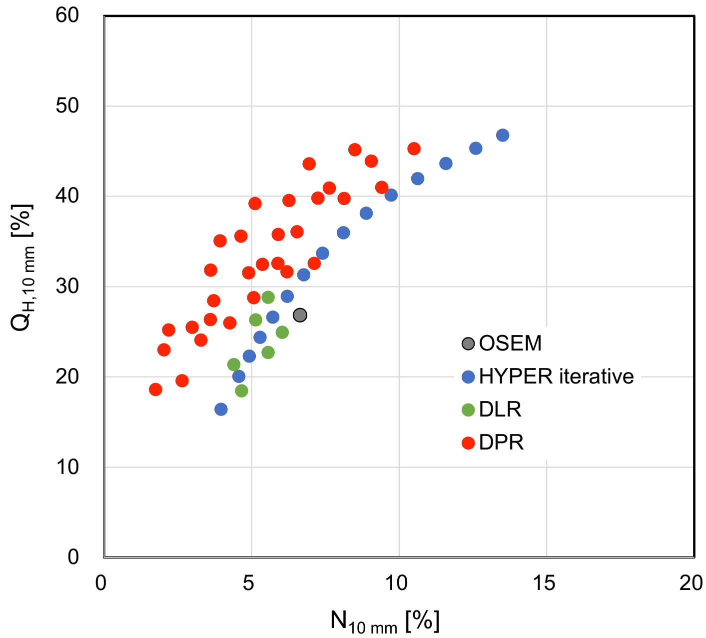

Figure 4. Relationship between % contrast and background variability for all reconstructed algorithms evaluated. OSEM represents OSEM + PSF + TOF.

Figure 5 shows PET images acquired for 2 min and reconstructed using various methods. Statistical noise in PET images was more apparent when OSEM + PSF + TOF was applied, but lower with HYPER DPR. Sphere detectability on PET images was visually better for HYPER DPR than the other types of algorithms evaluated.

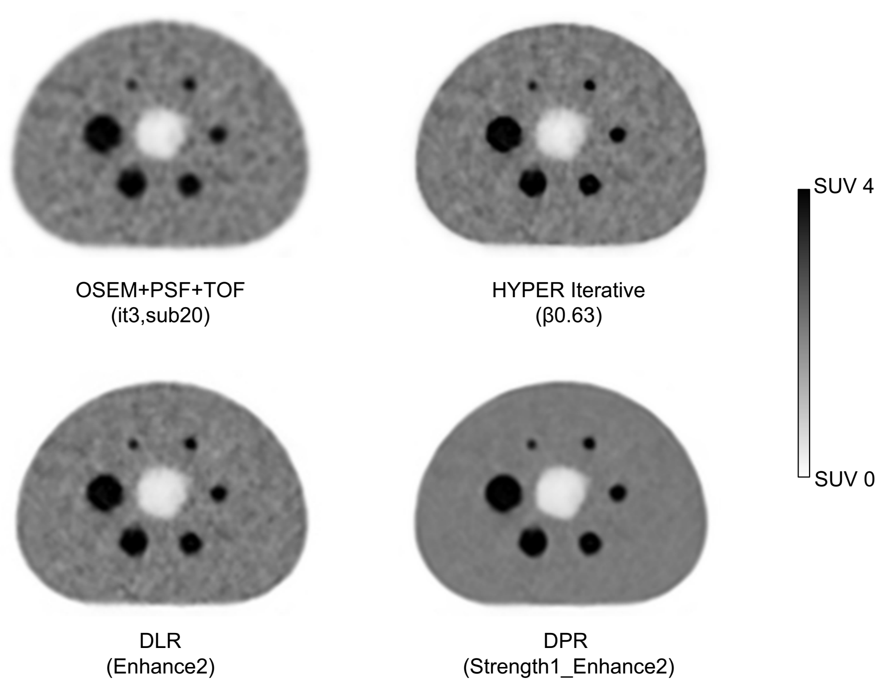

Figure 5. Examples of PET images reconstructed with OSEM +PSF +TOF (3 iterations; 20 subsets), HYPER Iterative (β = 0.63), HYPER DLR (Enhance2), and HYPER DPR (Strength1_Enhance2) acquired for the routine clinical duration of 2 min. The SBR was 4. All images are displayed as SUV on a scale of 0–4.

Figure 6 shows the SUV_{mean} and RC of hot spheres on images acquired for 10 min and reconstructed using OSEM (3 iterations; 20 subsets), HYPER Iterative (β = 0.63), DLR (Enhance2), and DPR (Strength1_Enhance2). The SUV_{mean} and RC differed considerably depending on the reconstruction method. Quantitation of 10 mm spheres was improved by HYPER Iterative, DLR and DPR. The tendency of sphere size dependence was similar among OSEM, HYPER DLR and HYPER DPR except for HYPER Iterative. The $SUV_{B,ave}$ of all reconstructions was within 0.95–1.05 (OSEM, 1.02; HYPER Iterative, 1.02–1.03; HYPER DLR, 1.02–1.03; HYPER DPR, 1.02–1.03). These results indicated that the scanner and reconstruction methods were appropriately calibrated, with quantitative accuracy within ± 5% error.

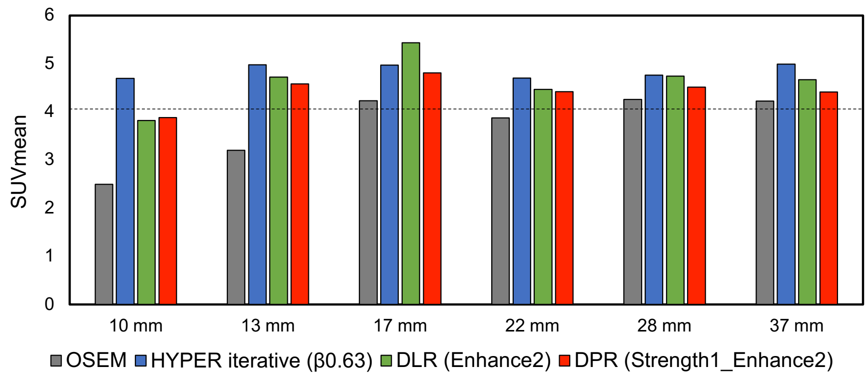

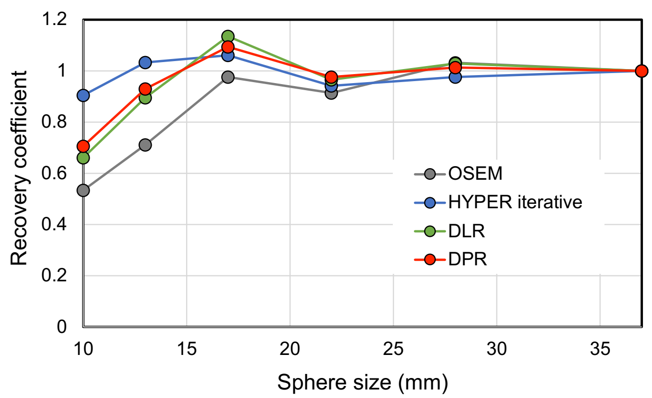

Figure 6. Results of SUV_{mean} and relative recovery coefficient of SUV_{mean} of hot spheres on images reconstructed with OSEM +PSF +TOF (3 iterations; 20 subsets), HYPER Iterative (β value, 0.63), HYPER DLR (Enhance2), and HYPER DPR (Strength1_Enhance2).

4. Conclusions

Our phantom results showed that the advanced image reconstruction algorithms can improve image quality and quantitative accuracy compared with traditional OSEM-based methods. In our evaluations, HYPER DPR reduced noise, improved image contrast, and enhanced PET image quantitation in 10 mm spheres, which may help improve detectability of smaller lesions. However, image quality and quantitation substantially differed according to the reconstruction parameters. The parameters of the new reconstruction methods may require optimization tailored to each institution and scanner, which will also be our next step. Further assessment using human data is needed to evaluate the performance of these advanced image reconstruction algorithms in various imaging scenarios.

5. Image/Figure Courtesy

All images are the courtesy of School of Health Sciences, Fukushima Medical University, Japan.

6. References

1. Miwa K, Wagatsuma K, Iimori T, Sawada K, Kamiya T, Sakurai M, et al. Multicenter study of quantitative PET system harmonization using NIST-traceable $^{68}Ge/^{68}Ga$ cross-calibration kit. Phys Med. 2018;52:98-103.
2. Akamatsu G, Shimada N, Matsumoto K, Daisaki H, Suzuki K, Watabe H, et al. New standards for phantom image quality and SUV harmonization range for multicenter oncology PET studies. Ann Nucl Med. 2022;36(2):144-61.
3. Chen S, Hu P, Gu Y, Yu H, Shi H. Performance characteristics of the digital uMI550 PET/CT system according to the NEMA NU2-2018 standard. EJNMMI Phys. 2020;7(1):43.
4. Japanese Society of Nuclear Medicine. Standard PET imaging protocols and phantom test procedures and criteria: executive summary. 2017: http://jsnm.org/wp_jsnm/wp-content/themes/theme_jsnm/doc/StandardPETProtocolPhantom20170201.pdf
5. Xing Y, Qiao W, Wang T, Wang Y, Li C, Lv Y, et al. Deep learning-assisted PET imaging achieves fast scan/low-dose examination. EJNMMI Phys. 2022;9(7).
6. Miwa K, Wagatsuma K, Nemoto R, Masubuchi M, Kamitaka Y, Yamao T, et al. Detection of sub-centimeter lesions using digital TOF-PET/CT system combined with Bayesian penalized likelihood reconstruction algorithm. Ann Nucl Med. 2020.
7. Yoshii T, Miwa K, Yamaguchi M, Shimada K, Wagatsuma K, Yamao T, et al. Optimization of a Bayesian penalized likelihood algorithm (Q.Clear) for ^{18}F-NaF bone PET/CT images acquired over shorter durations using a custom-designed phantom. EJNMMI Phys. 2020;7(1):56.

Author Biography

Dr. Kenta Miwa
Professor
Department of Radiological Sciences
School of Health Sciences, Fukushima Medical University, Fukushima, Japan

Kenta Miwa is a Professor of Radiological Sciences at Fukushima Medical University. He obtained his Bachelor of Health Science and Master of Medical Science degrees from Kitasato University, Japan, and his Ph.D. degree in Health Sciences from Kyushu University in 2015. He became an Assistant Professor of Radiological Sciences at Kyushu University, and then he moved to Fukushima Medical University in 2021. He has served the Japanese Society of Nuclear Medicine (JSNM), the Japanese Society of Nuclear Medicine Technology (JSNMT), the Society of Nuclear Medicine and Molecular Imaging (SNMMI), and the European Association of Nuclear Medicine (EANM) in several capacities.

PASSION for CHANGE

If you have any questions about the magazine, or simply wish to reach out to us for any other reasons, you are welcomed to contact us at the following email address: uinnovation-global@united-imaging.com